Polarization and intensity effects in two-photon dissociation of H_2 in two-frequency laser fields

Avijit Datta and S. S. Bhattacharyya
Atomic and Molecular Physics Section, Department of Materials Science, Indian Association for the Cultivation of Science, Jadavpur, Calcutta 700032, India

(Received 2 May 2000; published 17 January 2001)

We present a detailed calculation on $(1+1)$-photon resonance-enhanced photodissociation of molecular hydrogen. The first field of frequency ω_1 is tuned to excite the ground level $X\,^1\Sigma_g^+(v=0,j=0)$ to either one of the two strongly nonadiabatically coupled intermediate vibrational levels belonging to the electronic states $B\,^1\Sigma_u^+$ and $C\,^1\Pi_u$. These two levels can absorb a second photon of frequency ω_2 and connect to the continua of the $GK\,^1\Sigma_g^+$ and $I\,^1\Pi_g$ states as well as to the embedded discrete levels of the $H\bar{H}\,^1\Sigma_g^+$ and $J\,^1\Delta_g^+$ states. These embedded discrete levels predissociate into the continua of GK and I states. The differing transition amplitudes to the continua through the different pathways interfere, giving rise to a dissociation line shape as ω_2 is varied. The complex interplay between the mixture of bound and continuum states is reflected through this line shape. Further complexity is introduced by the radiative Raman-type coupling between the B and C state levels due to the second field. We have shown how the line shape changes with the change in relative polarizations of the two fields and their intensities in addition to the variable laser detuning. The polarization effects are very different depending on whether ω_2 is near resonance or off-resonance with the predissociating levels. The polarization dependence has been explained with reference to the variations in rotational factors of the matrix elements concerned and the consequent change in the dissociation amplitudes through different pathways. It has also been shown that the second field is much more effective than the first field as far as dissociation is concerned.

DOI: 10.1103/PhysRevA.63.023410 PACS number(s): 33.80.Wz, 33.80.Gj

I. INTRODUCTION

Multiphoton dissociation dynamics of small diatomic molecules in intense laser fields is of fundamental interest and has attracted much attention recently [1]. Dissociative processes in the region of moderately intense laser fields also have their own intrinsic interest as they may prove to be a convenient tool to explore nonadiabatic interaction between excited electronic states [2]. H_2 is the simplest molecule whose potential-energy curves and couplings between excited electronic states have been most thoroughly investigated both theoretically and experimentally [3–5]. In particular, double-resonance experiments have yielded energies of several high-lying levels, including the vibrational levels lying in the outer wells of excited electronic states [3]. These double-resonance experiments are similar to the situation described here. In spite of such extensive work, the spectroscopic properties of all the excited states of H_2 are not known in every detail. In particular, the above-mentioned nonadiabatic interactions between such states can be crucial in determining two-photon dissociation line shapes and angular distributions, as shown by early work of Siebbeles *et al.* [4].

Recently, with the aim of investigating these effects, we have theoretically investigated resonance-enhanced two-photon dissociation of H_2 from the ground $X\,^1\Sigma_g^+$ state to the final continua of the $GK\,^1\Sigma_g^+$ and $I\,^1\Pi_g$ electronic states for linear parallel polarizations of the two laser fields [2(b)]. Nondiabatic interactions between the electronic states in both the intermediate and final stages of the process were found to have an important bearing on the dissociation line shape. On or near resonance, the predissociating levels of the $J\,^1\Delta_g^+$ electronic state were found to play a crucial role, whereas the predissociating levels of the $H\bar{H}\,^1\Sigma_g^+$ electronic state did not affect the dissociation line shape significantly. Nonadiabatic mixing [5,7] between the two closely spaced intermediate resonant levels of the $B\,^1\Sigma_u^+$ and $C\,^1\Pi_u$ states was also reflected in the final dissociation line shape. The most recent and most accurate spectroscopic study of this aspect was made by Hinnen *et al.* [5(a)], where a deperturbation analysis was performed yielding a matrix element from which mixing can be determined. Here, with information on the energy-level structure of the excited state, we investigate the effects of different polarization and intensity combinations of the two laser fields on the dissociation line shape of the same process, i.e., the resonant two-photon dissociation of H_2 from the $X\,^1\Sigma_g^+(v=0,j=0)$ level through the predissociating levels belonging to the $J\,^1\Delta_g$ and $H\bar{H}\,^1\Sigma_g^+$ states to the continua of the GK and $I^{\pm}$ states. The intermediate resonance involved are the two nonadiabatically coupled, closely spaced levels $v=14,j=1$ of the $B\,^1\Sigma_u^+$ state and $v=3,j=1$ of the $C\,^1\Pi_u$ state [6]. The changes in polarization of the laser fields cause changes in the geometrical factors, arising from rotation, in various radiative matrix elements. These matrix elements enter into the description of the dissociation dynamics in different ways and mostly in a nonlinear fashion. They interfere with each other differently for different polarization combinations at particular fixed frequencies and intensities of the two fields. Thus we have found that the polarization dependence may give interesting insight into the nonadiabatic mixing of various levels. Here we present the dissociation line shapes for four polarization combinations; (i) linear-linear, (ii) circular-circular (same sense), (iii) circular-circular (opposite sense), and (iv) circular-linear of the two laser fields, for the fixed peak intensity combination $I_1{}^0=3.51\times10^8$ and $I_2{}^0=2.25\times10^6\ \mathrm{W\,cm^{-2}}$. We found that the polarization dependence may give interesting insight into

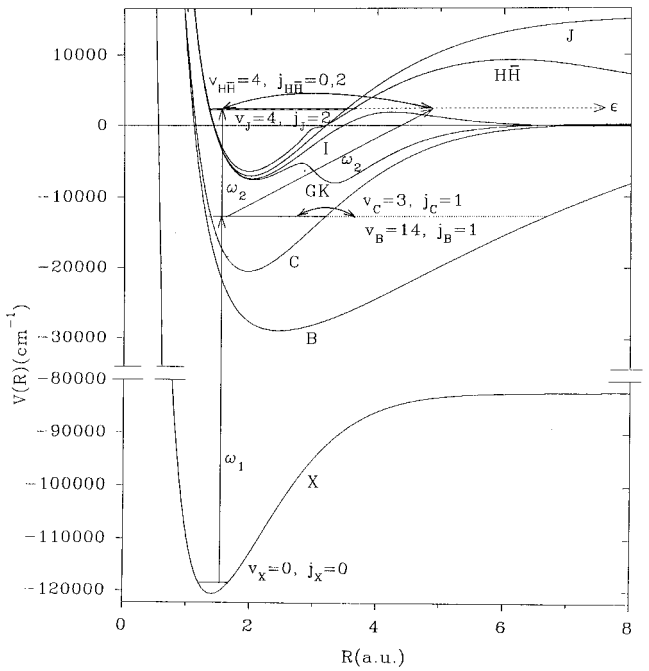

FIG. 1. Adiabatic potential energies $V(R)$ for the pertinent states of H_2. Excitations from the initial ground level of the X state to the two closely spaced nonadiabatically coupled intermediate levels of the B and C states and then dissociation to the final continua of GK and I states directly or through predissociating levels of $H\bar{H}/J$ states are shown schematically.

the nonadiabatic mixing of various levels. The relative intensity variations of the two laser fields for a fixed polarization combination (circular+linear) with changing Rabi frequencies have been studied for their effect on the dissociation line shape.

II. THEORY AND FORMULATION

The scheme for multiphoton dissociation of the H_2 molecule that we have considered here is shown in Fig. 1 on the pertinent potential-energy diagram. Molecules initially in the $v=0, j=0$ level of the ground $X\,^1\Sigma_g^+$ electronic state (which we have designated as $|0\rangle$) successively absorb two photons of frequency ω_1 and ω_2, and dissociate as $H(1s)+H(2s/2p)$, where v and j are the vibrational and rotational quantum numbers, respectively. The near-resonant intermediate levels that are coherently excited after absorption of a photon of frequency ω_1 are the $v=14$, $j=1$ level of the $B\,^1\Sigma_u^+$ electronic state, designated as $|1\rangle$, and the $v=3, j=1$ level of the $C\,^1\Pi_u$ electronic state, designated as $|2\rangle$. They have a separation of 17.2 cm^{-1} in the adiabatic Born-Oppenheimer approximation, but are strongly coupled through nonadiabatic (NA) interaction [7]. The laser of frequency ω_2 resonantly couples both levels $|1\rangle$ and $|2\rangle$ with the continua of $GK\,^1\Sigma_g^+$ and $I\,^1\Pi_g$ states, which we denote in general by $|\varepsilon\rangle$. The transition to the dissociative continuum of the $EF\,^1\Sigma_g^+$ state is negligible and has been neglected [2,8]. The range of frequency ω_2 is so chosen that from the intermediate levels $|1\rangle$ and $|2\rangle$, after absorption of a ω_2 photon, near resonance may occur with the bound rovibrational levels of the $H\bar{H}\,^1\Sigma_g^+$ state with $j=0$ and 2 and v either 4 or 5 (levels $|3\rangle$ and $|4\rangle$, respectively, in our notation) and also with the $j=2$ level of the $J\,^1\Delta_g^+$ state (level $|5\rangle$) and v either 4 or 5. These levels are embedded within the continua of the GK and I states and interact nonadiabatically with them to dissociate as $H(1s)+H(2s/2p)$. Thus additional pathways of H_2 photodissociation are provided via these predissociating (PD) levels. Other bound levels of the $H\bar{H}$ and J states, and the quasibound levels of the I state, which may act as predissociating levels, are highly off-resonant with $|1\rangle$ and $|2\rangle$, and are not effectively coupled to the intermediate levels by the photon of frequency ω_2. Hence they contribute insignificantly to the dissociation dynamic at the laser intensities we are interested in.

As the dissociation scheme considered in this paper is essentially the same as in our previous paper [2(b)], we present here only a brief outline of the formulation.

The time-dependent Schrödinger equation for the molecular system in the two-frequency laser fields is given by (in a.u.)

$$i\frac{\partial|\Psi\rangle}{\partial t}=H|\Psi\rangle=[H_{\rm mol}+\tilde{V}_{\rm rad}+\tilde{V}(t)+\tilde{V}_{\rm NA}]|\Psi\rangle. \quad (1)$$

$\tilde{V}_{\rm rad}$ and $\tilde{V}_{\rm NA}$ are the radiative and nonradiative interaction operators, which are time dependent and time independent, respectively.

The total wave function is expanded in the adiabatic basis as

$$|\Psi\rangle=\sum_n C_n(t)\exp(-iE_nt)|n\rangle+\sum_{j=1,2}\int C_{\varepsilon_j}(t)\times\exp(-\varepsilon_jt)|\varepsilon_j\rangle d\varepsilon_j, \quad (2)$$

where E_n is the energy of the nth level ($n=0-5$), and $|\varepsilon_j\rangle$ is the jth continuum state corresponding to an energy ε_j. The two continua (with $j=1,2$) considered here belong to the GK and I electronic states, respectively.

Putting $\tilde{V}=\tilde{V}_{\rm rad}(t)+\tilde{V}_{\rm NA}$, the equation of motion for the probability amplitudes in the base of the above five discrete states and the continua can be written as

$$\dot{C}_n(t)=-i\sum_m \tilde{V}_{nm}C_m(t)e^{i(E_n-E_m)t}-\sum_{j=1,2}\int \tilde{V}_{m\varepsilon_j}C_{\varepsilon_j}(t)e^{i(E_n-E_m)t}d\varepsilon_j, \quad (3)$$

where $\tilde{V}_{nm}=\langle m|\tilde{V}|n\rangle$ is the interaction matrix element between $|n\rangle$ and $|m\rangle$, which is time dependent for radiative interaction and time independent for NA interaction.

The radiative interaction is taken to arise from two classical pulsed laser fields E_1 and E_2, of frequencies ω_1 and ω_2, with different polarizations $\hat{\varepsilon}_1$ and $\hat{\varepsilon}_2$. Thus the total laser field is

$$\vec{E}(t)=E_1(t)\cos(\omega_1 t)\hat{\varepsilon}_1+E_2(t)\cos(\omega_2 t)\hat{\varepsilon}_2. \tag{4}$$

The field amplitudes $E_1(t)$ and $E_2(t)$ are both assumed to have a sine-squared time dependence with a pulse duration τ_p and pulse full width at half maximum $\tau_p/2$ [2,10], $E_1(t)=E_1^0\sin^2(\pi t/\tau_p)$ and $E_2(t)=E_2^0\sin^2(\pi t/\tau_p)$, where E_1^0 and E_2^0 are the peak amplitudes.

The bound-state $\Sigma/\Pi/\Delta$ wave functions, free-state Σ/Π wave functions, and time-independent electron-nuclear rotational matrix elements of the nonadiabatic coupled configuration-interaction Hamiltonian were defined in our previous paper [2(b)] in detail. The radiative interaction Hamiltonian in this case is

$$\tilde{V}_{\rm rad}=-\vec{E}(t)\cdot d=-[E_1(t)\cos(\omega_1 t)\hat{\varepsilon}_1\cdot\vec{d}+E_2(t)\cos(\omega_2 t)\hat{\varepsilon}_2\cdot\vec{d}], \tag{5}$$

where [9]

$$\hat{\varepsilon}\cdot\vec{d}=\sum_{\lambda=1}^{+1} d_\lambda D^{1*}_{p\lambda}(\phi,\theta,0)(1-2\delta_{p1}). \tag{6}$$

Here θ and ϕ are the directions of the internuclear axis with respect to the space-fixed Z axis. The peak amplitude E^0 and peak intensity I^0 are connected by the relation

$$I^0=\frac{c(E^0)^2}{8\pi}. \tag{7}$$

(where both I^0 and E^0 are in a.u.), i.e., $I^0=3.511\,89\times10^{16}\times(E^0)^2$ (where I^0 is expressed in W cm^{-2} and E^0 is expressed in a.u.). We indicate the polarization indices of the two fields of peak intensities ${I_1}^0$ of frequency ω_1 and ${I_2}^0$ of frequency ω_2 by p_1 and p_2, respectively. The polarization index is $p=0$ for parallel linear and $p=\pm1$ for the two senses of circular polarization. The four combinations of polarization (p_1 and p_2) we have used here are as follows.

(i) Both the fields are linearly polarized parallel to the space-fixed Z axis. For this case, only $\Delta M=0$ transitions are involved, where M is the projection of the angular momentum j on the space-fixed Z axis and polarization indices are $p_1=0,p_2=0$.

(ii) Both fields are circularly polarized in the same sense and the direction of propagation of both is parallel to the space-fixed Z axis; the polarization vector lies on the X-Y plane. For this case $\Delta M=1$ (or -1) will be involved and we take $p_1=1$ and $p_2=1$.

(iii) The same as the combination (ii), but the senses of polarization of the two circularly polarized fields are opposite to each other. Here $p_1=1$ and $p_2=-1$.

(iv) The field of frequency ω_1 is circularly polarized and is propagating parallel to the Z axis and the second field of frequency ω_2 is linearly polarized along this space-fixed Z axis (and hence is propagating in the space-fixed X-Y direction).

Using the corresponding values of p_1 and p_2 for the different polarizations we obtain the values of the matrix elements and the required parameters for our model. The radial parts of the matrix elements involved are independent of radiation field polarizations. However, the integration over the angular coordinates will give different radiative matrix elements for different polarizations. The relevant magnetic quantum numbers of the resonant intermediate levels and the final levels will be different for different polarization combinations. The expressions for the relevant radiative parameters (e.g., radiative widths and shifts of the intermediate levels) are evaluated from the bound-free matrix elements by integration over all the directions of motion in the continua.

The matrix element of the operator $\hat{\varepsilon}\cdot\overline{d}$ between any two bound levels (say, $g\rightarrow i$, characterized by quantum numbers j_i,M_i,Λ_i and j_g,M_g,Λ_g) can be written as (at a laser field $E=1$ a.u.)

$$\begin{aligned}\langle j_iM_i\Lambda_i|(\hat{\varepsilon}\cdot\vec{d})|j_gM_g\Lambda_g\rangle&=[(2j_i+1)(2j_g+1)]^{1/2}[(2-\delta_{\Lambda_i0})(2-\delta_{\Lambda_g0})]^{-1/2}\sum_\lambda(-1)^{p-\lambda}(-1)^{M_g-\Lambda_g}(1-2\delta_{p1})\\&\times\Bigg[\Bigg\{\begin{pmatrix}j_i,&1&j_g\\M_i&-p&-M_g\end{pmatrix}\Bigg\}+\begin{pmatrix}j_i&1&j_g\\\Lambda_i&-\lambda&-\Lambda_g\end{pmatrix}\pm(1-\delta_{\Lambda_g0})\begin{pmatrix}j_i&1&j_g\\M_i&-p&-M_g\end{pmatrix}\\&\times\begin{pmatrix}j_i&1&j_g\\\Lambda_i&-\lambda&\Lambda_g\end{pmatrix}\Bigg\}\pm(1-\delta_{\Lambda_i0})\Bigg\{\begin{pmatrix}j_i&1&j_g\\M_i&-p&-M_g\end{pmatrix}\begin{pmatrix}j_i&1&j_g\\-\Lambda_i&-\lambda&-\Lambda_g\end{pmatrix}\pm(1-\delta_{\Lambda_g0})\\&\times\begin{pmatrix}j_i&1&j_g\\M_i&-p&-M_g\end{pmatrix}\begin{pmatrix}j_i&1&j_g\\-\Lambda_i&-\lambda&\Lambda_g\end{pmatrix}\Bigg\}\Bigg]Q_{\Lambda_i,v_i,j_i;\Lambda_g,v_g,j_g;}(\lambda)\\&=(\text{angular part})\times(\text{radial part}),\end{aligned} \tag{8}$$

where we have defined $Q_{\Lambda_i,v_i;j_i,\Lambda_g,v_g,j_g;}(\lambda)=\int_R R^*_{\Lambda_i,v_i,j_i}(R)Q^\lambda_{\Lambda_i\Lambda_g}R_{\Lambda_g,v_g,j_g}(R)R^2dR$ as the radial part of any bound-bound matrix element and the rest is the angular part (or factor). Again, $Q^\lambda_{\Lambda_i,\Lambda_g}(R)=\int_R\Psi^*_{\Lambda_i}(\vec{r}_e,R)d_\lambda(\vec{r}_e,R)\Psi_{\Lambda_g}(\vec{r}_e,R)d\vec{r}_e$ are the electronic transition moments between two states Λ_g and Λ_i, $\vec{r}_e$ and R are the electronic and relative nuclear coordinates, respectively, and d_λ is the dipole moment operator.

The transition matrix element between any intermediate bound level and a continuum state (say, $i \rightarrow f$) can be written as (at a laser field $E=1$ a.u.)

$$\langle j_f M_f \Lambda_f | (\hat{\varepsilon}\cdot\vec{d}) | j_i M_i \Lambda_i \rangle = \left[\frac{(2j_f+1)}{4\pi}\right]\left[\frac{(2j_i+1)}{4\pi}\right]^{1/2} (-i)^{j_f} e^{i\delta_{j_f}} (2-\delta_{\Lambda_f 0})^{-1/2} (2-\delta_{\Lambda_i 0})^{-1/2}$$
$$\times \sum_{\lambda} (-1)^{p-\lambda} (-1)^{M_i-\Lambda_i} (1-2\delta_{p1}) \int_{\theta,\phi} [[D^{j_f}_{M_f\Lambda_f}(\phi,\theta,0) D^{j_f}_{M_f\Lambda_f}(\phi_k,\theta_k,0)$$
$$\pm (1-\delta_{\Lambda_f 0}) D^{j_f}_{M_f-\Lambda_f}(\phi,\theta,0) D^{j_f}_{M_f-\Lambda_f}(\phi_k,\theta_k,0)]$$
$$\times D^{1}_{-p,-\lambda}[D^{j_i}_{-M_i-\Lambda_i}(\phi,\theta,0) \pm (1-\delta_{\Lambda_i 0}) D^{j_i}_{-M_i\Lambda_i}(\phi,\theta,0)] \sin\theta\, d\theta\, d\phi] Q_{\Lambda_f v_f, j_f:\Lambda_i, v_i, j_i:}(\lambda), \quad (9)$$

where $Q_{\Lambda_f, v_f: j_f, \lambda_i, v_i, j_i:}(\lambda)$ is defined as the radial part of any bound-free matrix element and the rest is the angular part (or factor) of the bound-free matrix element.

As shown in our previous paper [2(b)], we can obtain seven coupled differential equations using the rotating-wave approximation, considering only the resonant and near-resonant terms. Continuum states can then be eliminated from the basis set expansion of the Schrödinger equation and, using the Markov approximation [11], the problem is formulated in terms of a set of six coupled differential equations involving only the resonant discrete and quasidiscrete levels:

$$\dot{C}_0(t) = -iC_1(t)V_{01}(t)e^{-i\Delta_{10}t} - iC_2(t)V_{02}(t)e^{-i\Delta_{20}t}, \quad (10a)$$

$$\dot{C}_1(t) = -iV_{12}C_2(t)e^{i\delta_{12}t} - iV_{13}(t)C_3(t)e^{i\Delta_{13}t}$$
$$-iV_{14}(t)C_4(t)e^{i\Delta_{14}t} - iV_{10}(t)C_0(t)e^{i\Delta_{10}t} - C_1(t)$$
$$\times[\tfrac{1}{2}\gamma_{11} + is_{11}] - C_2(t)[\tfrac{1}{2}\gamma_{12} + is_{12}]e^{i\delta_{12}t} - C_3(t)$$
$$\times[\tfrac{1}{2}\gamma_{13} + is_{13}]e^{i\Delta_{13}t} - C_4(t)[\tfrac{1}{2}\gamma_{14} + is_{14}]e^{i\Delta_{14}t}$$
$$-C_5(t)[\tfrac{1}{2}\gamma_{15} + is_{15}]e^{i\Delta_{15}t}, \quad (10b)$$

$$\dot{C}_2(t) = -iV_{21}C_1(t)e^{-i\delta_{12}t} - iV_{23}(t)C_3(t)e^{i\Delta_{23}t}$$
$$-iV_{24}(t)C_4(t)e^{i\Delta_{24}t} - iV_{25}(t)C_5(t)e^{i\Delta_{25}t}$$
$$-iV_{20}(t)C_0(t)e^{i\Delta_{20}t} - C_1(t)[\tfrac{1}{2}\gamma_{21} + is_{21}]e^{-i\delta_{12}t}$$
$$-C_2(t)[\tfrac{1}{2}\gamma_{22} + is_{22}] - C_3(t)[\tfrac{1}{2}\gamma_{23} + is_{23}]e^{i\Delta_{23}t}$$
$$-C_4(t)[\tfrac{1}{2}\gamma_{24} + is_{24}]e^{i\Delta_{24}t} - C_5(t)$$
$$\times[\tfrac{1}{2}\gamma_{25} + is_{25}]e^{i\Delta_{25}t}, \quad (10c)$$

$$\dot{C}_3(t) = -iV_{31}(t)C_1(t)e^{-i\Delta_{13}t} - iV_{32}(t)C_2(t)e^{-i\Delta_{23}t} - C_1(t)$$
$$\times[\tfrac{1}{2}\gamma_{31} + is_{31}]e^{-i\Delta_{13}t} - C_2(t)[\tfrac{1}{2}\gamma_{32} + is_{32}]e^{-i\Delta_{23}t}$$
$$-C_3(t)[\tfrac{1}{2}\gamma_{33} + is_{33}], \quad (10d)$$

$$\dot{C}_4(t) = -iV_{41}(t)C_1(t)e^{-i\Delta_{14}t} - iV_{42}(t)C_2(t)e^{-i\Delta_{24}t} - C_1(t)$$
$$\times[\tfrac{1}{2}\gamma_{41} + is_{41}]e^{-i\Delta_{14}t} - C_2(t)[\tfrac{1}{2}\gamma_{42} + is_{42}]e^{-i\Delta_{24}t}$$
$$-C_4(t)[\tfrac{1}{2}\gamma_{44} + is_{44}], \quad (10e)$$

$$\dot{C}_5(t) = -iV_{52}(t)C_2(t)e^{-i\Delta_{25}t} - C_1(t)[\tfrac{1}{2}\gamma_{51} + is_{51}]e^{-i\Delta_{15}t}$$
$$-C_2(t)[\tfrac{1}{2}\gamma_{52} + is_{52}]e^{-i\Delta_{25}t} - C_5(t)[\tfrac{1}{2}\gamma_{55} + is_{55}], \quad (10f)$$

where $\Delta_{i0} = E_i - E_o - \omega_1$, $\Delta_{ik} = E_i - E_k + \omega_2$, $\delta_{il} = E_i - E_l$, $\delta_{k\varepsilon_j} = E_k - \varepsilon_j$ $(i,l=1,2$ and $k=3,4,5,\varepsilon_j)$, $\tilde{V}_{01} = V_{01}e^{i\omega_1 t}$, $\tilde{V}_{13} = V_{13}e^{i\omega_2 t}$, $\tilde{V}_{1\varepsilon_f} = V_{1\varepsilon_f}e^{i\omega_2 t}$, $\tilde{V}_{12} = V_{12}$, $\tilde{V}_{3\varepsilon_f} = V_{3\varepsilon_f}$, etc.,

$$\gamma_{nm} = 2\pi \sum_{j=1,2} \int V_{n\varepsilon_j} V^*_{\varepsilon_j m} \delta(E'_n - \varepsilon_j) d\varepsilon_j, \quad (11a)$$

and

$$s_{nm} = \sum_{j=1,2} \mathrm{P} \int \frac{V_{n\varepsilon_j} V^*_{\varepsilon_j m}}{E'_n - \varepsilon_j} d\varepsilon_j, \quad (11b)$$

where $E'_n = E_n + \omega_2$ for $n=1,2$ and $E'_n = E_n$ for $n=3,4,5$. P indicates the principal value part of the integral.

The diagonal elements with $m=n$ for $n=1,2$ represent the linewidths (γ_{11} and γ_{22}) and shifts (s_{11} and s_{22}) of the levels $|1\rangle$ and $|2\rangle$ due to their radiative interactions $V_{n\varepsilon_j} = \tilde{V}_{n\varepsilon_j}e^{-i\omega_2 t}$ with the continua of the GK and I states. These linewidths and shifts are time dependent, since they depend upon the laser field intensities. The off-diagonal elements s_{12} and γ_{12} represent the real and imaginary parts, respectively, of the Raman-like coupling terms between the two levels $|1\rangle$ and $|2\rangle$ introduced by the field of frequency ω_2. The diagonal elements for $m=n=3,4,5$ give the field-independent (and hence time-independent) linewidths (γ_{nn}) and shifts (s_{nn}) of the levels $|3\rangle$, $|4\rangle$, and $|5\rangle$ arising from their NA interactions $V_{n\varepsilon_j} = \tilde{V}_{n\varepsilon_j}$ with the continua of GK and I states.

TABLE I. Radial parts of the matrix elements of the dipole moment operator between different radiatively interacting bound levels.

State	Radial part	
X-B	0.182 03	
X-C^+	−0.291 98	
B-$H\bar{H}(v=4)$	$j=0$	$j=2$
	0.031 62	0.030 58
C^+-$H\bar{H}(v=4)$	$j=0$	$j=2$
	−0.030 32	−0.074 72
C^+-$J^+(v=4)$	0.558 29	
B-$H\bar{H}(v=5)$	$j=0$	$j=2$
	−0.037 43	−0.037 33
C^+-$H\bar{H}(v=5)$	$j=0$	$j=2$
	−0.153 13	−0.140 416
C^+-$J^+(v=5)$	−0.149 47	

The off-diagonal elements s_{1n}, s_{2n}, and γ_{1n}, γ_{2n} with $n=3,4,5$ give the real and imaginary parts of the radiative-nonadiabatic mixed terms.

Equations (10a)–(10f) are solved numerically using the fourth-order Runge-Kutta method [12] by imposing the initial condition $C_0=1$ and $C_1=C_2=C_3=C_4=C_5=0$ at $t=0$. From the populations $|C_n(t)|^2$ of the different levels $|n\rangle$ $(n=0-5)$, the dissociation probability $P(t)$ at any time t can be calculated as

$$P(t)=1-\sum_{n=0}^{5}|C_n(t)|^2. \tag{12}$$

The mode of calculation of the parameters from data available in the literature has been discussed in our previous paper [2(b)].

III. RESULTS AND DISCUSSION

As in the earlier work [2(b)], the six predissociating levels considered in this work have been divided into two groups. The first group (designated as group 1) contains the three PD levels $v=4$, $j=0$ and 2 of the $H\bar{H}$ state and $v=4$, $j=2$ of the J state, while the second group (designated as group 2) contains the other three PD levels $v=5$, $j=0$ and 2 of the $H\bar{H}$ state and $v=5$, $j=2$ of the J state. As the second frequency ω_2 is varied, the final continuum energy increases from below the group-1 PD levels to above the group-2 PD levels.

The direction of the space-fixed Z axis, the direction of the polarization vectors with respect to this axis, and the selection rules for the magnetic quantum number have been discussed earlier. In Tables I and II, we have listed the radial and angular parts, respectively, of the allowed radiative interaction matrix elements between the bound levels. While the radial parts are polarization independent, the angular factors are different for different polarizations of the two laser fields. The polarization of the ω_1 photon only is involved in the transition matrix element between the initial level and the bound levels belonging to B and C states. In the case of transition from these intermediate bound levels to the PD levels, the transition matrix elements depend on both the polarizations since the polarization of ω_1 determines the intermediate m state (m representing the magnetic quantum number) from which the transition occurs. This m depen-

TABLE II. Angular factors involved for different bound-bound radiative transitions for different polarizations of the two laser fields. (The two indices denote the j and M quantum numbers respectively.)

State	Circular-linear (+1,0)	Same-sense circular (+1,+1)	Opposite-sense circular (+1,−1)		Linear parallel (0,0)	
X-B	$-\frac{1}{\sqrt{3}}$ (0,0)→(1,1)	$-\frac{1}{\sqrt{3}}$ (0,0)→(1,1)	$-\frac{1}{\sqrt{3}}$ (0,0)→(1,1)		$\frac{1}{\sqrt{3}}$ (0,0)→(1,0)	
X-C^+	$-\frac{\sqrt{2}}{\sqrt{3}}$ (0,0)→(1,1)	$-\frac{\sqrt{2}}{\sqrt{3}}$ (0,0)→(1,1)	$-\frac{\sqrt{2}}{\sqrt{3}}$ (0,0)→(1,1)		$\frac{\sqrt{2}}{\sqrt{3}}$ (0,0)→(1,0)	
B-$H\bar{H}$	$\frac{1}{\sqrt{5}}$ (1,1)→(2,1)	$-\frac{\sqrt{2}}{\sqrt{5}}$ (1,1)→(2,2)	$\frac{1}{\sqrt{15}}$ (1,1)→(2,0)	$-\frac{1}{\sqrt{3}}$ (1,1)→(0,0)	$\frac{2}{\sqrt{15}}$ (1,0)→(2,0)	$\frac{1}{\sqrt{3}}$ (1,0)→(0,0)
C^+-$H\bar{H}$	$\frac{1}{\sqrt{10}}$ (1,1)→(2,1)	$-\frac{1}{\sqrt{5}}$ (1,1)→(2,2)	$\frac{1}{\sqrt{30}}$ (1,1)→(2,0)	$\frac{\sqrt{2}}{\sqrt{3}}$ (1,1)→(0,0)	$\frac{\sqrt{2}}{\sqrt{15}}$ (1,0)→(2,0)	$-\frac{\sqrt{2}}{\sqrt{3}}$ (1,0)→(0,0)
C^+-J^+	$\frac{\sqrt{3}}{\sqrt{10}}$ (1,1)→(2,1)	$-\frac{\sqrt{3}}{\sqrt{5}}$ (1,1)→(2,2)	$\frac{1}{\sqrt{10}}$ (1,1)→(2,0)		$\frac{\sqrt{2}}{\sqrt{5}}$ (1,0)→(2,0)	

dence causes the intermediate bound-PD level matrix elements to be different for different combinations of polarization. In Table III, we have listed angular factors for all radiative bound-free matrix elements that arise for different polarization combinations of the two laser fields. The peak intensities of the two laser fields have been kept fixed at $I_1^0 = 3.50\times10^8$ and $I_2^0 = 2.25\times10^6$ W cm^{-2} in this calculation. The rest of the required parameters are the same as in the previous paper [2(b)].

In Fig. 2, we have plotted the radial parts of all the useful bound-free matrix elements against the kinetic energy of the dissociated fragments. We note that for both *B*-*GK* and *C*-*GK* transitions, the matrix elements for $j=0$ and 2 of the *GK* state are nearly equal in magnitude but opposite in sign. This is a general phenomenon observed in work with either H_2^+ or HD^+. The extrema in the *B*-*GK* matrix elements are at the continuum energy position 3411 cm^{-1}. The radial part of the *C*-*GK*($j=0,2$) bound-free matrix element decreases almost linearly in absolute value with increase in continuum energy in the region shown. The radial matrix element of the *B*-*I*($j=2$) bound-free transition varies with energy in an oscillatory manner as shown in the figure. On the other hand, the radial part of the matrix element of *C*-*I*($j=2$) first decreases to a minimum value at continuum energy 2195 cm^{-1} and then decreases in magnitude continuously with increase in continuum energy.

The NA interaction between the two electronic states *B* and *C* mixes the two close-lying levels $|1\rangle$ and $|2\rangle$, i.e., $v=14$ and $j=1$ of $B\,{}^1\Sigma_u^+$ and $v=3$ and $j=1$ of ${}^1\Sigma_u^+$ states so

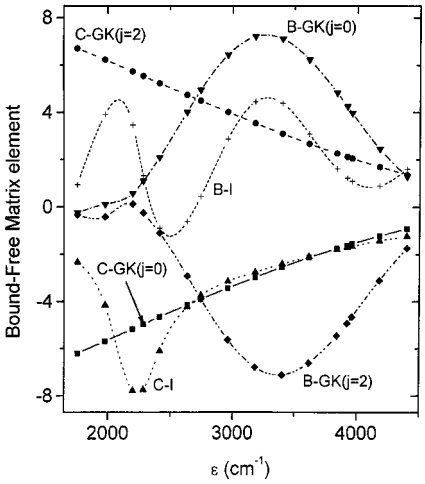

FIG. 2. Variations of the radial parts of the matrix elements of intermediate bound levels to free levels of the continua with the continuum energy ε measured from the dissociation threshold of the *GK*/*I* electronic state.

that two new perturbed eigenstates with mixed Σ^+ and Π^+ character are created. These two perturbed eigenstates are denoted as the perturbed *B* and perturbed *C* states. They have about 73% *B* character (and 27% *C* character) and 73% *C* character (and 27% *B* character), respectively [2(b)].

In Figs. 3(a)–3(d), we show the dissociation probability as a function of the second frequency ω_2 for four different combinations of polarization of the two laser fields at differ-

TABLE III. (Angular factor)×(complex conjugate of angular factor) for different bound-free radiative transitions for different polarization combinations of the two laser fields.

	(Angular factor)×(complex conjugate of angular factor)					
State	Circular-linear (+1,0)	Same-sense circular (+1,+1)	Opposite-sense circular (+1,−1)	Linear parallel (0,0)		
B-*GK*	$\frac{1}{5}$ (1,1)→(2,1)	$\frac{2}{5}$ (1,1)→(2,2)	$\frac{1}{15}$ (1,1)→(2,0)	$\frac{1}{3}$ (1,1)→(0,0)	$\frac{4}{15}$ (1,0)→(2,0)	$\frac{1}{3}$ (1,0)→(0,0)
B-I^+	$\frac{3}{20}$ (1,1)→(2,1)	$\frac{3}{10}$ (1,1)→(2,2)	$\frac{1}{20}$ (1,1)→(2,0)		$\frac{2}{5}$ (1,0)→(2,0)	
B-I^-	$\frac{1}{4}$ (1,1)→(1,1)		$\frac{1}{4}$ (1,1)→(2,0)			
C^+*GK*	$\frac{1}{10}$ (1,1)→(2,1)	$\frac{1}{5}$ (1,1)→(2,2)	$\frac{1}{30}$ (1,1)→(2,0)	$\frac{2}{3}$ (1,1)→(0,0)	$\frac{2}{15}$ (1,0)→(2,0)	$\frac{2}{3}$ (1,0)→(0,0)
C^+-I^+	$\frac{3}{40}$ (1,1)→(2,1)	$\frac{3}{20}$ (1,1)→(2,2)	$\frac{1}{40}$ (1,1)→(2,0)		$\frac{1}{5}$ (1,0)→(2,0)	
C^+-I^-	$\frac{1}{8}$ (1,1)→(1,1)		$\frac{1}{8}$ (1,1)→(1,0)			

ent fixed values of frequency ω_1. The first field of frequency $\omega_1 = 105\,694$ and $105\,689$ cm^{-1} creates on resonance and near resonance with the perturbed B level in Fig. 3(a) and Fig. 3(c), respectively. Again, $\omega_1 = 105\,663$ and $105\,669$ cm^{-1} produce on resonance and near resonance with the perturbed level of the C state in Fig. 3(b) and Fig. 3(d), respectively. The perturbed B level has 73% B character and 27% C character due to strong nonadiabatic mixing between the unperturbed $B(v=14,j=1)$ and $C(v=3,j=1)$ levels, whereas the perturbed C level has 73% C state character and 27% B state character for the same reason. At the middle range of frequency ω_2, the predissociating levels are far off resonance and direct dissociation to the continua of the GK and I states from the intermediate levels of the B and C states is the only possible path. An important and significant difference in dissociation probability due to the change in polarization of the two laser fields is obtained in this range of ω_2 although the peak intensities of the two laser fields remain fixed at $I_1{}^0 = 3.51\times10^8$ and $I_2{}^0 = 2.25\times10^6$ W cm^{-2}.

As shown in Fig. 3(a), for far off-resonant excitation by

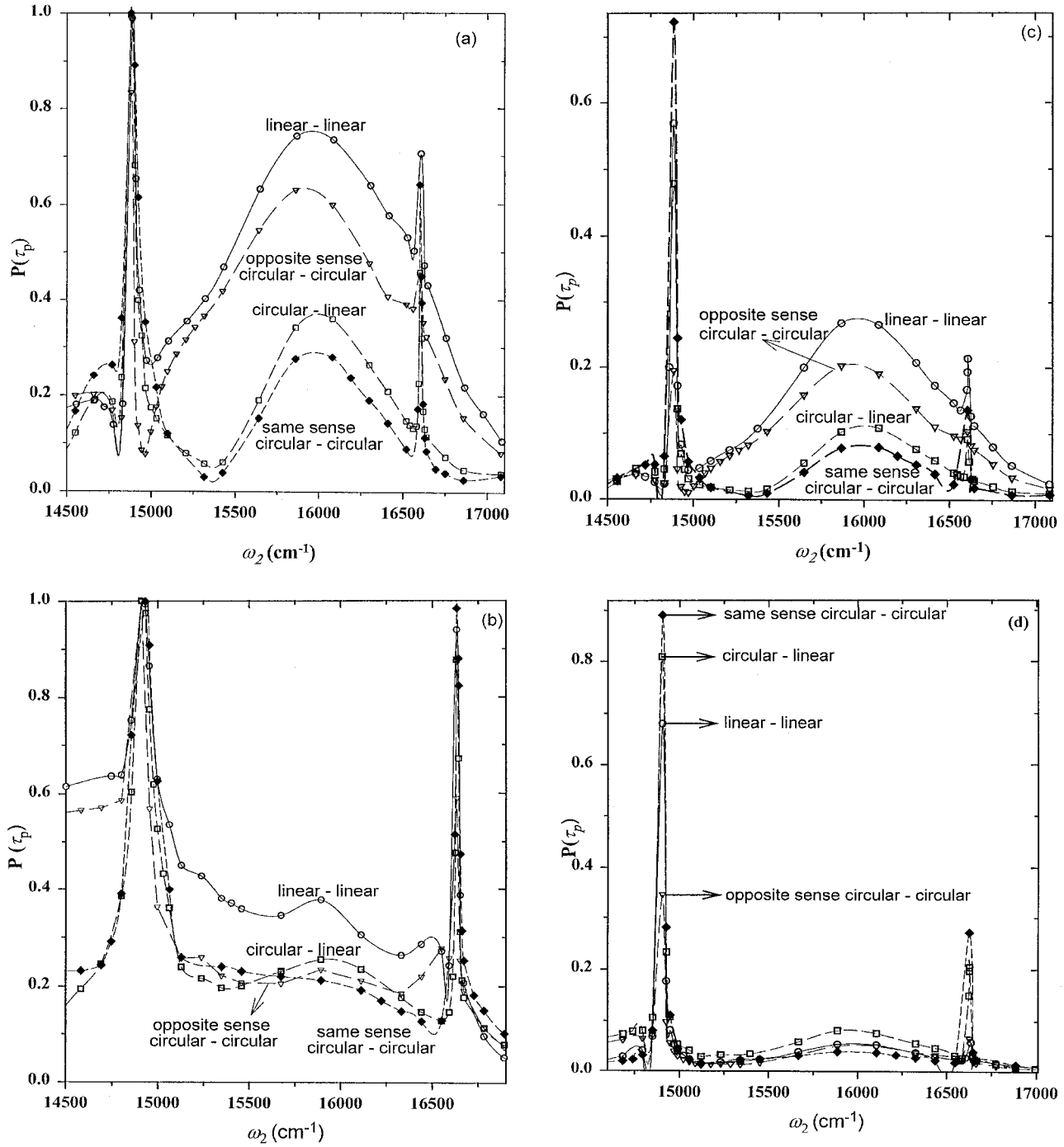

FIG. 3. Dissociation probability $P(\tau_p)$ against ω_2 for $\omega_1 =$ (a) 105 694, (b) 105 663, (c) 105 698, (d) 105 669 cm^{-1}, for four polarization combinations of the two laser fields.

the second frequency, the linear-linear and circular-circular, same-sense polarization combinations give the highest and lowest dissociation probabilities, respectively. Circular-linear and opposite-sense circular-circular polarization combinations have intermediate values, the latter being greater than the former. We see from Fig. 2 that B-$GK(j=0)$ and B-$GK(j=2)$ transitions have larger radial parts of the bound-free matrix elements than the other transitions in this region. B-$I^{\pm}$ bound-free matrix elements also have considerable magnitude of the radial part. Since the intermediate perturbed level of the B state has 73% B character, at this middle range of frequency ω_2 all the above four matrix elements should contribute significantly in Fig. 3(a). The highest value of dissociation probability for the linear-linear polarization combination in this region is due to the considerably larger values of the angular factors for all the relevant matrix elements for this combination compared to the other polarization combinations. For the opposite-sense circular-circular polarization, the degenerate I^- state becomes accessible from the intermediate state and hence opposite-sense circular-circular polarization combinations have four dissociative paths B-$GK(j=0)$, B-$GK(j=2)$, B-I^+, and B-I^-. Again, the matrix elements of B-$GK(j=0)$ and B-I^- have large values of the angular factor. So the opposite-sense circular-circular polarization combination gives a large dissociation probability, although it is lower than the linear-linear polarization combination, in spite of the fact that the B-I^- path is radiatively forbidden for linear-linear polarization. Same-sense circular-circular polarization has the lowest dissociation probability due to low values of the angular factors of B-GK and B-I^+ matrix elements. Circular-linear polarization gives a slightly higher dissociation probability than same-sense circular-circular polarization, mainly due to the extra path B-I^-, which is forbidden for same-sense polarization.

In Fig. 3(b), the intermediate resonance occurs with the perturbed C level (with 73% C character) by absorption of a photon of frequency ω_1. Since the matrix elements of B-GK and B-I transitions have larger values than those for C-GK and C-I transitions, in this case the magnitude of the dissociation probability is smaller than in the preceding case. Since most of the angular factors of the matrix elements for linear-linear polarization have larger values than for other polarization combinations, it again gives the largest dissociation probability as in Fig. 3(a). For other sets of polarization, variation of all the radial and angular parts of all the matrix elements gives comparable resultant dissociation probabilities. Since at the middle range of frequency ω_2 the resultant dissociation is due to the net effects of all the matrix elements and the matrix elements themselves vary nonlinearly with energy, these line shapes can intersect each other for different polarization combinations of the two laser fields, as seen in Fig. 3(b). This is made more complicated by the fact that the dissociation through the I^- state is radiatively allowed for circular-linear and opposite-sense circular-circular polarizations but forbidden for the other two polarization combinations.

The first field of frequency ω_1 has been made slightly off resonant with the perturbed level of the B state in Fig. 3(c). At the middle range of frequency ω_2, comparative values of the dissociation probability for different polarization combinations show the same features as those in Fig. 3(a), where ω_1 was on resonance with the perturbed level of the B state. At near resonance with group-2 predissociating levels the ordering for different polarization combinations remains the same as that in Fig. 3(a). For near resonance with the group-1 predissociating levels the peak values of the dissociation probability are in decreasing magnitude for same-sense circular-circular, linear-linear, circular-linear, and opposite-sense circular-circular polarization combinations. These features are same as for near resonance with group-2 predissociating levels in Fig. 3(b) for intermediate resonance with the perturbed level of the C state by the first field of frequency ω_1.

For near resonance with the perturbed level of the C state by the first field of frequency ω_1, we notice from Fig. 3(d) that at the middle range of frequency ω_2 the ordering of dissociation probability magnitudes is quite similar to that of Fig. 3(b). The ordering of the peak values of the dissociation probabilities at near resonance with the group-1 and group-2 predissociating levels shows the same features as those of Figs. 3(c) and 3(b), respectively.

Thus, at on resonance and near resonance with the predissociating levels, some features, in particular the ordering of the peak heights, are changed from those obtained when the second frequency has no resonance with any PD level. Polarization change of the laser fields affects the line shape because of a change in angular factors of the intermediate bound to predissociating bound matrix elements, or of the intermediate bound to free matrix elements, or both. In Figs. 4(a) and 4(b), we have magnified the portions of the dissociation line shapes of Figs. 3(a) and 3(b) that are on and near resonance with the two groups of predissociating levels.

Figure 4(a) shows the near-resonant line shapes with the two groups of predissociating levels for intermediate resonance with the perturbed level of the B state. In the region of resonance with the group-2 predissociating levels, the intermediate level of the B state has an appreciable radiative width and so direct radiative dissociation and dissociation via predissociating levels both contribute considerably to the dissociation probability. The 27% unperturbed C character of this level and dominance of the J-I predissociation cause the matrix element for C-J transition also to play an important part in determining the dissociation probability, which is also consistent with the results of our previous work [2(b)]. Thus, a change of the angular factor of the matrix element of the C-J transition for different polarizations changes the dissociation probability for the predissociating path. Same-sense circular-circular polarization has a larger angular factor of the C-J matrix element than linear-linear polarization. This factor induces strong predissociative decay for same-sense circular-circular polarization. But direct dissociation is much more facilitated for linear-linear polarization than for all three other polarization combinations. The resultant of the two processes gives a higher peak value for linear-linear than for same-sense circular-circular polarization. Although opposite-sense circular-circular polarization should cause a large direct radiative decay, the angular factor of the C-J

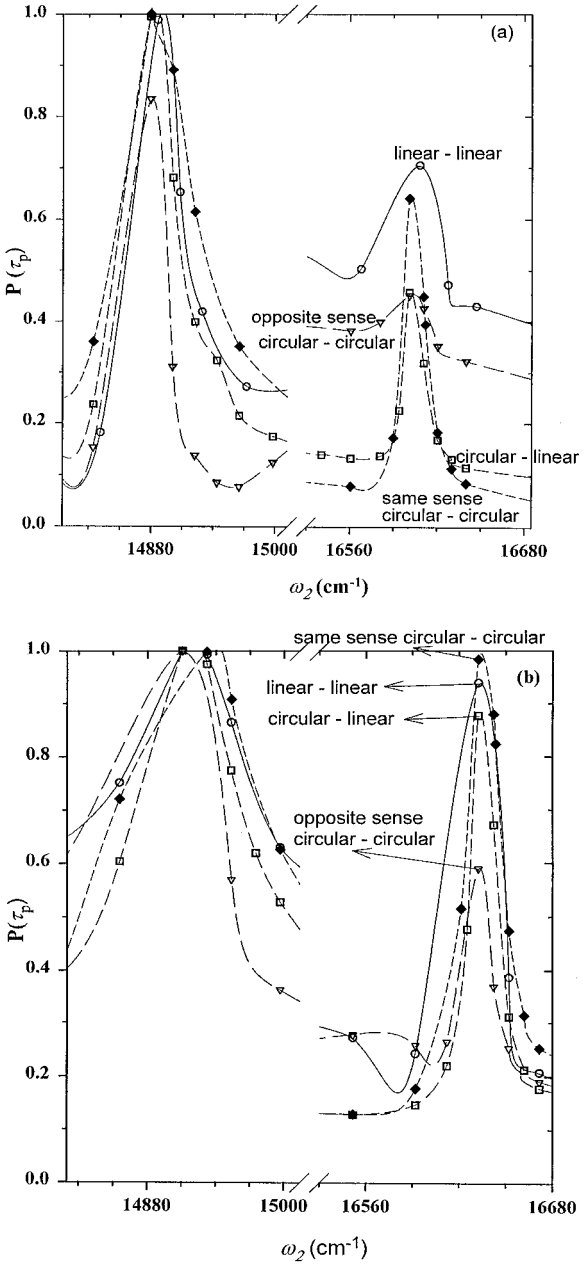

FIG. 4. Dissociation probability $P(\tau_p)$ against ω_2 for near-resonance positions of the two groups of predissociating levels for $\omega_1 =$ (a) 105 694, (b) 105 663 cm^{-1}, for four polarization combinations of the two laser fields.

matrix element for this polarization combination is very small. The resultant gives a small peak because of the feeble predissociating effect. The angular factor of the C-J matrix element for circular-linear polarization has an appreciable value, which results in a considerable increase in the dissociation probability for this combination due to the presence of predissociating effects. At exact resonance with the group-1 predissociating levels, the dissociation probabilities for all the polarization combinations except opposite-sense circular-circular polarization reach unity, because C-J matrix elements are huge and total saturation occurs through the PD path. The opposite-sense circular-circular polarization combination has the lowest dissociation probability, which does not saturate due to the low angular factor of the C-J matrix element. Since the perturbed B level has 27% C character and the unperturbed C level has large radiative width at the position of the group-1 predissociating levels, the dissociation probability around group-1 predissociating levels is higher than around the group-2 predissociating levels.

The dissociation line shapes at near resonance with the two groups of predissociating levels for intermediate resonance with the perturbed level of the C state by the first field of frequency ω_1 are shown in Fig. 4(b). Now at near-resonance positions with the group-2 predissociating levels, predissociating paths dominate over direct dissociation channels, since here the radiative width of the unperturbed level of the C state is very small. Thus, the structures are determined almost solely by the different angular factors of the C-J matrix elements for different polarization combinations. On resonance, same-sense circular-circular polarization gives the highest dissociation probability due to the highest angular factor of the C-J matrix element. Opposite-sense circular-circular polarization gives the lowest dissociation probability on resonance for the corresponding reason. The linear-linear and circular-linear polarization combinations give values in between, due to intermediate values of the angular factors for these polarization combinations. Of these two, the values for the linear-linear polarization are slightly higher. At on or near resonance with the group-1 predissociating levels both direct radiative decay from the intermediate level of the C state and dissociation via the PD levels contribute significantly to the dissociation probability. However, the angular factor of the C-J matrix element and the angular factors of the bound-free matrix elements determining predissociative and direct radiative dissociation change with the change in polarization in different ways. Thus, the various polarization combinations give different line-shape structures whose widths are sensitive to the polarization combination. In the region of near resonance with the group-1 predissociating levels, the widths of the peaks of the dissociation line shapes of Fig. 4(b) are much larger than those of Fig. 4(a), since perturbed intermediate levels of the C state have 73% unperturbed C character, with large radiative width in this range of frequencies.

In Figs. 5(a) and 5(b), we have plotted the dissociation line shapes with variation of the frequency ω_2 for a circular-linear polarization combination of the two laser fields for two fixed frequencies of ω_1 on resonance with the perturbed levels of the B and C states, respectively. Here we have considered five intensity combinations of the two laser fields to obtain their relative intensity effects on the dissociation probability. In both figures at the middle range of frequency ω_2 we notice that the intensity of the second field of frequency ω_2 has a much more pronounced enhancement effect on the dissociation probability compared to the intensity of the first field of frequency ω_1. In Fig. 5(a), where resonance occurs with the intermediate perturbed level of the B state, at the middle range of frequency ω_2, the dissociation probabilities are much higher than the probabilities at corresponding frequencies in Fig. 5(b) where the perturbed level of the C state is on resonance with the field of frequency ω_1. This is

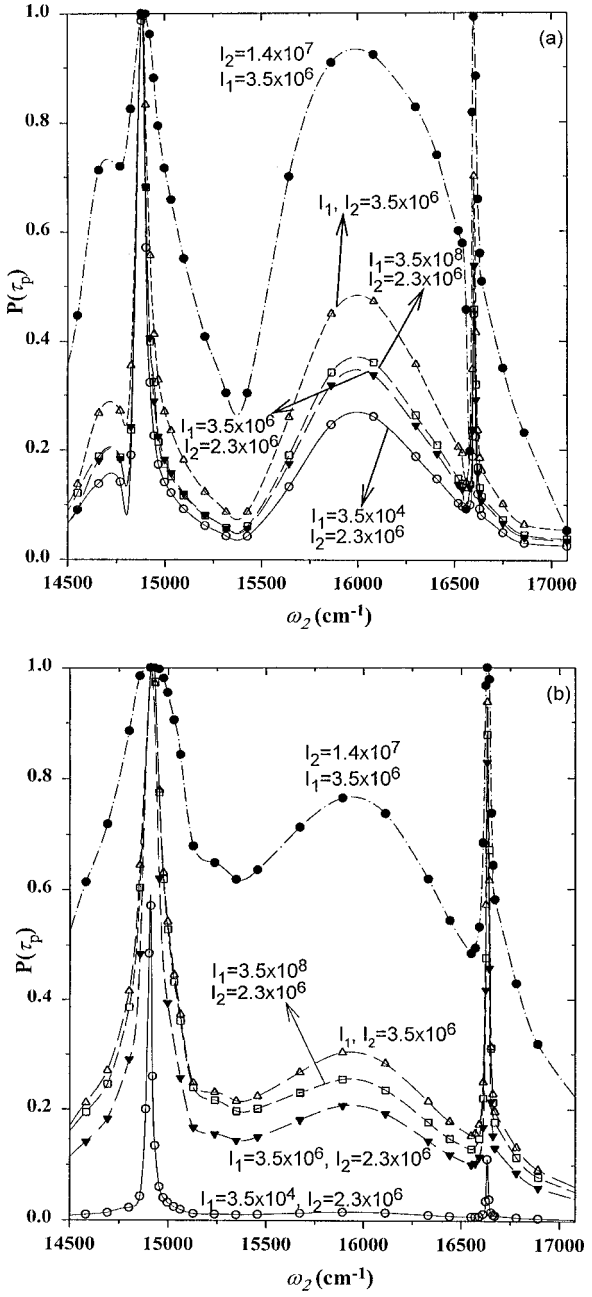

FIG. 5. Dissociation probability $P(\tau_p)$ against ω_2 for ω_1 = (a) 105 694, (b) 105 663 cm^{-1}, for different peak intensity combinations of the two laser fields. I_i are the peak intensities in W cm^{-2}.

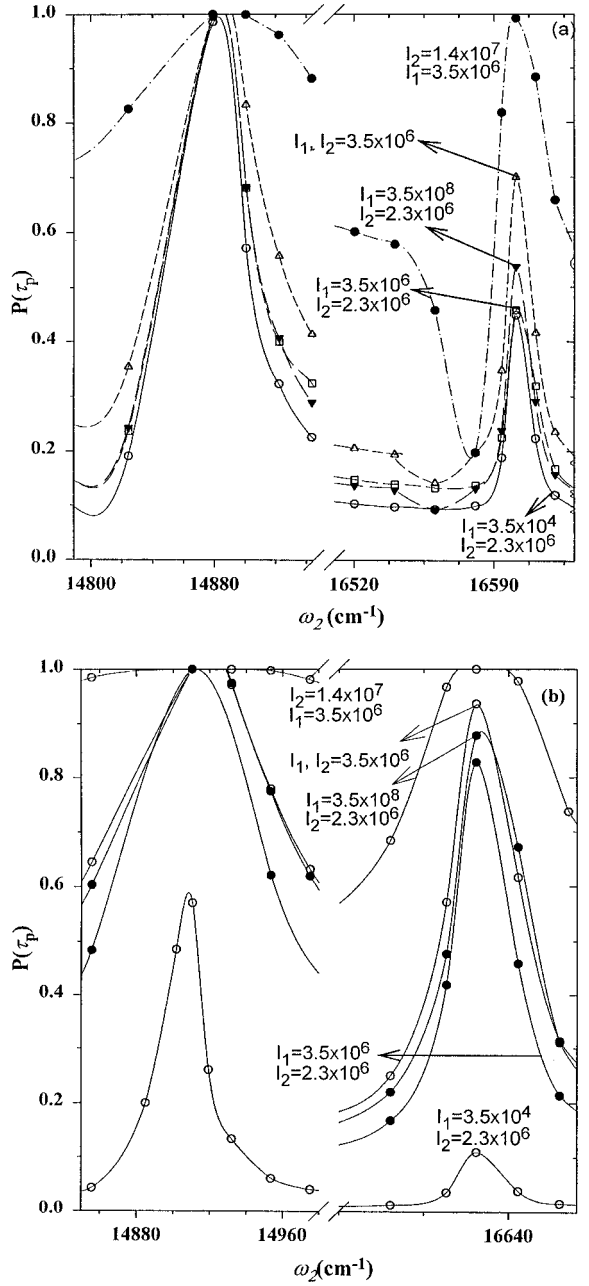

FIG. 6. Dissociation probability $P(\tau_p)$ against ω_2 for near-resonance positions of the two groups of predissociating levels for ω_1 = (a) 105 694, (b) 105 663 cm^{-1}, for different peak intensity combinations of the two laser fields. I_i are the peak intensities in W cm^{-2}.

because for this range of ω_2 radiative widths of the unperturbed level of the B state have large values.

At on or near resonance with the predissociating levels, the intensity effects are more interesting due to the simultaneous contribution of nonadiabatic and radiative decay to the continua. The resultant dissociative line shape is due to the interference among all these nonadiabatic and direct radiative decay paths.

In Figs. 6(a) and 6(b), we have plotted the dissociation probabilities at on or near resonance with the two groups of predissociating states. Here, due to the variation of intensities of the two laser fields, the radiative matrix elements change, causing change in the resultant structure of the dissociation line shape. In Fig. 6(a), for resonance with the two groups of predissociating levels we notice that a rise in intensity of the first field, keeping $I_2{}^0$ fixed at 2.25×10^6 W cm^{-2}, does not change the dissociation probability much, whereas rise in intensity of the second field keeping the first field intensity fixed at $I_1{}^0 = 3.51\times10^6$ W cm^{-2} changes the line shape considerably. There is a particularly notable change for intensity $I_2{}^0 = 1.41\times10^7$ W cm^{-2}. This is due to the fact that the second

field interacts with the continua and continuum-embedded predissociating levels, but the first field does not. A similar feature is also visible in Fig. 6(b).

IV. CONCLUSIONS

We have presented polarization and intensity effects on the resonance-enhanced two-photon dissociation of H_2 in a two-frequency field where nonadiabatic interactions play crucial roles in the dissociation dynamics. Our calculation has taken into account the complex interplay between the bound and continuum states due to radiative and nonradiative interactions. This demonstrates that the interference between different pathways leading to resonant multiphoton dissociation gives rise to complicated variations of the dissociation line shape with the polarizations of the lasers concerned. The specific features of the process obtained in our case are as follows.

(i) At far from resonance in the second step, where predissociating levels do not contribute to the dissociation line shape, the relative magnitudes of the dissociation probability for different polarization combinations are determined mainly by the bound-free matrix elements. The radial parts of these matrix elements at a particular kinetic energy are different for the bound levels of B and C states. In general, matrix elements from both these levels are involved in the dynamics due to their nonadiabatic mixing. For fixed values of intensities $I_1{}^0=3.51\times10^8$ and $I_2{}^0=2.25\times10^6\,\mathrm{W\,cm^{-2}}$, the dissociation probability interestingly varies greatly for different polarizations of the two laser fields when intermediate resonance with the perturbed level of the B state is achieved by the first field of frequency ω_1. On resonance with the perturbed level of the C state, the variation is somewhat less. This difference is because in the two cases the bound-free matrix elements from the bound levels of the B and C states are involved differently. In both cases, the linear-linear polarization combination gives much higher dissociation probability compared to the other polarization combinations. These results can be explained in terms of the different angular factors involved in each radiative matrix element due to the change in polarizations of the two laser fields.

(ii) Completely different polarization dependence of the dissociation line shape is obtained on or near resonance, and far from resonance, of the predissociating levels with the second field of frequency ω_2. On or near resonance with the predissociating levels, nonadiabatic decay of $H\bar{H}$ and J electronic states and direct radiative dissociation both contribute in general to the dissociation process. But one of these effects can dominate over the other, depending on the polarization combination of the two fields. It is interesting to note that decay through these predissociating levels largely depends on field polarizations. Due to the strong Franck-Condon overlap between the wave functions of C and J states, the C-J matrix elements play a more important role in the dissociation process than B-$H\bar{H}$ and C-$H\bar{H}$ matrix elements. Thus the variation of angular factor of the C-J matrix element with changing polarizations of the two laser fields explains most of the variation of nonadiabatic predissociation for near resonance with the two groups of predissociating levels. Again, dissociation through the electronic state I^- is forbidden for certain polarization combinations but allowed for others. This also causes a relative change of the dissociation probabilities when the polarizations are changed.

(iii) We also see that intensity variation of the second field causes more drastic changes in the dissociation probability than variation in the first field. It is interesting to note that, at the lowest intensity of the first field used, on-resonance excitation of only one of the intermediate perturbed levels can cause complete dissociation, and only when one of the two groups of predissociating levels is excited.

Of course, the laser parameters used in the calculation cannot be presently obtained in standard off-the-shelf lasers. This makes the experimental use of such pulses with the proposed parameters rather difficult. However, we would like to point out that the parameters are not very far from those of state-of-the-art lasers, thus making such experiments at least conceivable. In particular, this kind of intensity profile for the first VUV frequency field may be available in the near future allowing experiments on this type of systems. Also, interesting experiments [13] on the polarization dependence of different dissociative ionization channels of simple molecules in intense fields have begun very recently. Some of the results show very different polarization dependence in different channels. Although our work does not cover intense-field effects, one plausible explanation becomes evident from this work. It might be possible that, for different polarizations, different intermediate levels are involved as dominant resonances and each of these levels has different angular factors in the matrix elements involved in the transition for different polarizations. Thus, it would be of great interest to investigate the possibilities of exploring complicated intramolecular dynamics in the presence of strong fields, through multiphoton processes. These calculations could be of importance in such situations.

[1] A. Giusti-Suzor, F. H. Mies, L. F. DiMauro, E. Charron, and B. Yang, J. Phys. B **28**, 309 (1995).

[2] (a) S. Banerjee, S. S. Bhattacharyya, and S. Saha, Phys. Rev. A **49**, 1836 (1994); (b) A. Datta, S. Saha, and S. S. Bhattacharyya, *ibid.* **61**, 1324 (1999).

[3] W. L. Glab and J. P. Hessler, Phys. Rev. A **35**, 2102 (1987); E. Reinhold, W. Hogervorst, and W. Ubachs, Phys. Rev. Lett. **78**, 2543 (1997); E. Reinhold, A. De Lange, and W. Ubachs, J. Chem. Phys. **109**, 9772 (1998).

[4] (a) L. D. A. Siebbeles, J. M. Schins, W. J. van der Zande, J. A. Beswick, and N. Halberstadt, Phys. Rev. A **45**, 4481 (1992); (b) L. D. A. Siebbeles, J. M. Schins, W. J. van der Zande, J. Los, and M. Glass-Maujean, *ibid.* **44**, 343 (1991).

[5] (a) P. C. Hinnen, W. Hogervorst, S. Stolte, and W. Ubachs,

Phys. Rev. A **72**, 1032 (1994); (b) L. Wolniewicz and K. Dressler, J. Chem. Phys. **88**, 3861 (1988).
[6] S. Banerjee, S. S. Bhattacharyya, and S. Saha, J. Raman Spectrosc. **24**, 317 (1993); S. Ghosh, S. S. Bhattacharyya, and S. Saha, J. Chem. Phys. **107**, 5332 (1997).
[7] P. S. Julienne, Mol. Phys. **48**, 508 (1973); A. L. Ford, J. Mol. Spectrosc. **53**, 364 (1974).
[8] S. Banerjee, M. K. Chakrabarty, S. S. Bhattacharyya, and S. Saha, J. Chem. Phys. **95**, 1608 (1991); **96**, 4974 (1992).
[9] B. Datta and S. S. Bhattacharyya, Phys. Rev. A **48**, 2153 (1993).
[10] M. Protopapas and P. L. Knight, J. Phys. B **28**, 4459 (1995).
[11] W. Heitler, *Quantum Theory of Radiation* (Clarendon, Oxford, 1954).
[12] W. H. Press, S. A. Teukolsky, W. T. Vetterling, and B. P. Flannery, *Numerical Recipes in Fortran* (Cambridge University Press, Cambridge, 1992), p. 70.
[13] S. Banerjee, G. Ravindra Kumar, and D. Mathur, Phys. Rev. A **60**, R25 (1999).